



Modelling the mechanical entrainment of metal droplets by solid particles in liquid slags

Ir. Inge Bellemans^a, prof. dr. ir. Nele Moelans^b, prof. dr. ir. Kim Verbeken^a

^a Ghent University

Department of Materials Science and Engineering

Technologiepark, 903

B-9052 Zwijnaarde (Ghent), Belgium

^b KU Leuven

Department of Materials Engineering

Kasteelpark Arenberg 44, box 2450

B-3001 Heverlee (Leuven), Belgium

Abstract

A variety of pyrometallurgical industries encounters production losses due to the mechanical entrainment of metallic droplets, i.e. the droplets are attached to solid particles in slags. The attached metal cannot settle, decreasing the efficiency of the phase separation. This results in inadequate decantation and eventually production losses in e.g. industrial Cu smelters and Pb reduction melting furnaces.

Recent experimental results on this interaction indicate the importance of interfacial energies. Simulations can give a more systematic insight into the observed phenomenon and the phase field modelling technique is well-suited for modelling microstructural evolution. In the present work, a phase field model describes a solid-liquid binary system with spinodal decomposition in the liquid near a non-reacting solid particle.

The influence of the interfacial energies and the particle morphology on the attachment of metallic droplets to solid particles was investigated. Depending on the relative magnitudes of the interfacial energies, four different regimes were found, namely, non-wetting, low wettability, high wettability and full wettability.

In the case of full or high wettability, the perimeter of the particle determines the amount of attached metal. Moreover, the space available around the particle, determined by the shape and proximity of other particles, can restrict the amount of attached metal. In practice, fewer but larger solid particles close to each other would provide less attached metal and thus a better phase separation.



1. Introduction

Metal extraction is based on the distribution of metals and impurities between two or more phases of which at least one contains a high concentration of the desired metal, for example by the reduction of Fe-rich ore, steel is made in a blast furnace. The distribution of the main metals and impurities between the phases is based on thermodynamic laws and therefore driven by composition, temperature, atmosphere, etc. Apart from the chemical distribution, the metals can only be recovered if a physical distribution also occurs. Here, a major issue is the entrainment of metal droplets in the oxide phase due to physical interactions between droplets and solid particles present in the liquid slag. This attachment creates production losses in industrial Cu smelters [1], Pb reduction melting furnaces [2] and other industries.

As mentioned above, these metal-oxide systems are influenced by composition, temperature, atmosphere, etc. To improve phase separations, the fundamental mechanisms governing the attachment of metal droplets to solid particles in liquid slags need to be identified which would require many experiments to investigate the influence of all parameters. Experimental investigation of this interaction has only started recently [3]. Consequently, available experimental results are scarce. However, the first experiments indicated that interfacial energies play an important role. The microstructure and composition of the phases can be investigated microscopically, but it is not straightforward to reveal the underlying chemical and physical phenomena as an experimental study of the effect of an individual parameter is very difficult, because it is almost impossible to keep the others constant.

Modelling can assist in gaining understanding of the evolution of microstructures and gives a more systematic insight into the role of some material properties. The physical and chemical properties of the system are well-controlled and the effect of each property can be investigated separately. The phase field method is a very powerful and versatile modelling technique for microstructural evolution. It was already used to model solidification [4], [5], solid-state phase transformations [6] and solid-state sintering [7].

In the phase field method, microstructures are represented by a set of field variables that are continuous functions of space and time. At interfaces, the field variables vary smoothly between the equilibrium values in the neighbouring grains. The position of the boundaries as a function of time is implicitly given by the field variables. This method avoids the mathematically difficult problems of applying boundary conditions at an interface whose position is part of the unknown solution. The phase field equations are derived from an energy functional according to thermodynamic principles. [8]

The model in this work and in [9], [10] describes a hypothetical system and is used to simulate the growth of liquid metal droplets (formed due to spinodal decomposition and indicated by the variation in the metal fraction [11]–[13]) in an oxide melt with dispersed solid oxide particles (indicated with a phase field variable and assumed to be nonreactive). The influence of the interfacial tensions



and the size, shape and number of the solid particles on the behaviour of the liquid metal droplets is investigated.

First, the formulation of the model is presented, then the numerical implementation and simulation parameters are introduced. After which the results are presented and discussed and these are finally summarized at the end.

2. Model formulation

This work introduces a model to describe the droplet formation and growth in the presence of solid particles. The combination of a non-conserved phase-field variable ϕ and a conserved composition field x_M enables the description of the microstructural evolution of an isothermal hypothetical binary O-M (oxide-metal) system at constant pressure. ϕ is used to distinguish between the liquid phases ($\phi=0$) and the solid particle ($\phi=1$) and x_M represents the local molar fraction of the metallic element M. Both variables are position- and time-dependent and the position of the boundaries between the different phases is implicitly given by them, i.e. the variables continuously change from one bulk value to another bulk value over the interface. [8]

It is assumed that the concentration of the solute in the precipitate is fixed and the molar volume V_m is the same in both phases and does not depend on composition. Moreover, convection is not included.

2.1. Evolution equations

The microstructure evolution is driven by minimization of the total Gibbs energy. The evolution of the conserved variable is governed by the following mass balance equation

$$\frac{\partial x_M}{\partial t} = \nabla \cdot [M \nabla [(1 - h(\phi))f'_{Liquid}(x_M) + h(\phi)f'_{Solid}(x_M) - \kappa_{x_M} \nabla^2 x_M]] \quad (1)$$

The coefficient M ($\text{m}^5 / (\text{J s})$) is related to the interdiffusion coefficient D of the liquid as $D = A_{Sp}M$. κ_{x_M} is the gradient energy coefficient for the liquid-liquid interfaces.

$f_{Solid}(x_M) = \frac{A_S}{2}(x_M - x_S)^2$ represents the bulk contribution of the solid phase. x_S and A_S (J/m^3) are model parameters that determine the position of the minimum and the steepness of the parabola, describing the Gibbs energies as a function of the molar fraction of metal.

Analogously, $f_{Liquid}(x_M) = \frac{A_{Sp}}{2}(x_M - x_{eq,LO})^2(x_M - x_{eq,LM})^2$ represents the homogeneous part of the free energy of the liquid phase. The corresponding free energy curve has a slope of A_{Sp} and two minima at $x_{eq,LO}$ and $x_{eq,LM}$. Where oxidic liquid (slag) is indicated with 'LO', and metallic liquid with 'LM'. Initially, the uniform supersaturation of the oxidic liquid is x_i , but this liquid decomposes spinodally into the two equilibrium compositions corresponding to the minima in the free energy

curve. Fluctuations are required to initiate spinodal decomposition: a random noise term, from a normal distribution with mean 0 and standard deviation 0.001, is added in every 100th time step. Figure 1 displays the free energy curves of the liquid and solid phases.

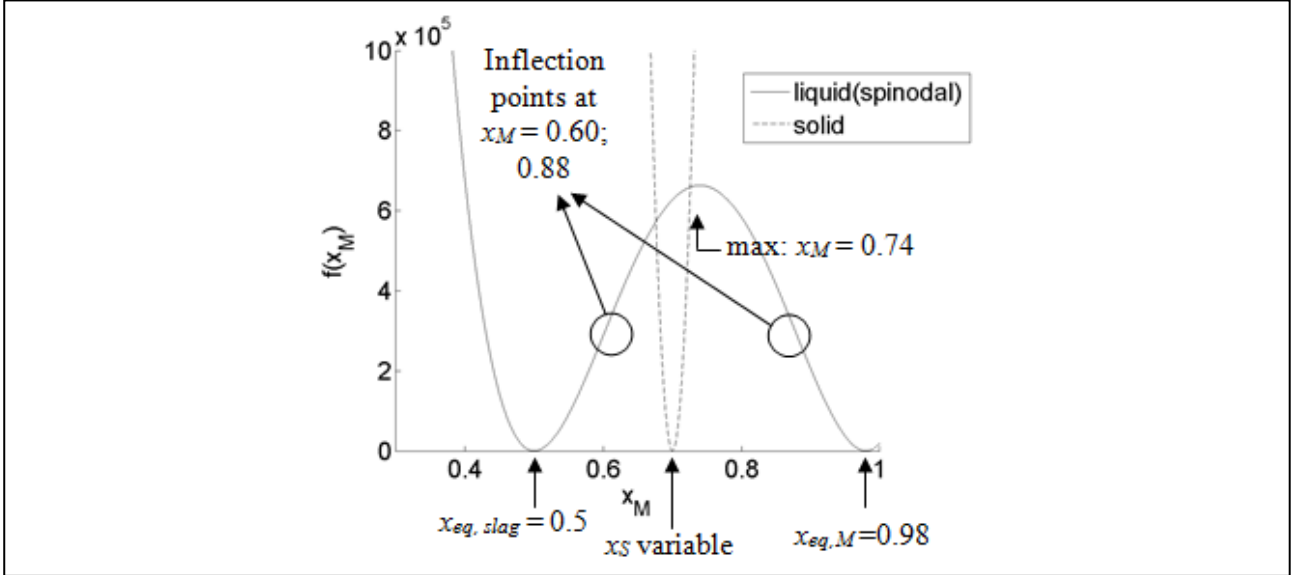


Figure 1: Free energy curves of the liquid (spinodal) and solid phases as a function of the mole fraction of metal M (here, for a solid phase with a fixed mole fraction of 0.70)

The interpolation function $h(\phi)$ has the form $h(\phi) = \phi^3(10 - 15\phi + 6\phi^2)$. With $h(\phi = 1) = 1$ in the solid and $h(\phi = 0) = 0$ in the liquid.

The non-conserved phase field variable ϕ evolves according to the following equation [14]

$$\frac{\partial \phi}{\partial t} = -L \frac{\delta F}{\delta \phi} = -L [W g'(\phi) + h'(\phi)(f_{\text{solid}} - f_{\text{liquid}}) - \kappa_{\phi} \nabla^2 \phi] \quad (2)$$

Where W is the depth of the double well function and κ the gradient energy coefficient for the solid-liquid interfaces.

2.2. Interface properties

Two types of interfaces are present: solid - liquid and liquid oxide - liquid metal. Both types are diffuse due to the gradient terms in the total energy expression. Following the approach of Cahn and Hilliard [12], the expression of the interfacial energy (J/m²) of the liquid-liquid interface $\gamma_{LO,LM}$ is:

$$\gamma_{LO,LM} = \frac{1}{6} \sqrt{\kappa_{x_M} A_{Sp}} (x_{eq,LM} - x_{eq,LO})^3 \quad (3)$$

Especially noteworthy about this model is the expression for the solid-liquid interfacial energy (J/m²) $\gamma_{S,Lk}$ (with $k = O$ or M , when the oxide or the metal liquid is involved, respectively) as it consists of two contributions,



$$\gamma_{S,LO} \text{ or } \gamma_{S,LM} = \frac{1}{3\sqrt{2}} \sqrt{W\kappa_\phi} + \gamma_{S,Lk}^{\nabla x_M} \quad (4)$$

The first term arises following the approach of Allen and Cahn [14] and the second term from the fact that a solid-liquid interface implies a change in both the phase field variable ϕ and the compositional variable x_M across the solid-liquid interface, yielding a non-zero gradient term for x_M . This contribution cannot be evaluated analytically. Thus, the following assumption was made: the composition dependence of the Gibbs energy across the interface is approximated by a spinodal function.

$$\frac{0.5(A_{Sp}+A_S)}{2} (x_M - x_S)^2 (x_M - x_{eq,Lk})^2 \quad (5)$$

This gives,

$$\gamma_{S,Lk}^{\nabla x_M} \approx \frac{1}{6} \sqrt{\kappa_{x_M} 0.5(A_{Sp} + A_S) (|x_S - x_{eq,Lk}|)^3} \quad (6)$$

2.3. Constant parameters

In this study, a hypothetical O-M system is considered and as the model parameters can be linked with physical system properties, a typical order of magnitude was chosen for most parameters. The model parameters are listed in Table 1.

Table 1: Values and descriptions of several constant parameters in the model

Model parameters		
Symbol	Description	Value(s)
N	System size	[256 256 1] grid points
Δx	Grid spacing	$(4/\sqrt{10}) 10^{-7}$ m
Δt	Time steps spacing	10^{-4} s
$x_{eq,LO}$	Equilibrium compositions of free energy curve of spinodal	0.50
$x_{eq,LM}$	decomposition	0.98
A_{Sp}	Steepness of free energy curve of spinodal decomposition	$4 \cdot 10^8$ J/m ³
A_S	Steepness of free energy curve of solid	$20 \cdot 10^8$ J/m ³
W	Depth of the double well function	$15 \cdot 10^6$ J/m ³
κ_ϕ	Gradient energy coefficient for the solid-liquid interfaces	$(15/8) \cdot 10^6$ J/m
L	Kinetic coefficient for the evolution of ϕ	10^{-30} m ³ /(J s)
$L_{initial}$	Kinetic coefficient for the evolution of ϕ for the first 1000 time steps	10^{-7} m ³ /(J s)
κ_{x_M}	Gradient energy coefficient for the liquid-liquid interfaces	$6 \cdot 10^{-6}$ J/m
M	Mobility coefficient of the metal	10^{-19} m ⁵ /(J s)

According to literature [15], [16], $\gamma_{LO,LM}$ is of the order of 1 N/m. Furthermore, the interfaces should at least contain five grid points for a sufficient resolution of the diffuse transitions at interfaces and



to reproduce accurately the surface energies [17]. With the values mentioned in Table 1, the liquid-liquid interfacial energy possesses the following constant value: $\gamma_{LO,LM} = 0.9030$ N/m. And the interfacial widths possess the following values for all simulations: $l_{LO,LM} = 8.0687$ grid points and $l_{S,LO} = 7.9057$ grid points for the interface between solid and liquid oxide and $l_{S,LM} = 7.9057$ grid points for the interface between solid and liquid metal. M is chosen such that the diffusion coefficient $D = 4 \cdot 10^{-11}$ m²/s. It is assumed that the particle does not transform, providing a very small value of L .

Experimentally observed solid particles in slags have dimensions of the order of μm [3]. In the simulations the particle size of a single large rectangular particle is taken as 100 by 50 grid points, corresponding to 12.65 by 6.32 μm . For a system size of 256 by 256 grid points, corresponding to 32.38 by 32.38 μm , the particle volume fraction is thus 0.0763. In reality, large variations are found (from 2-6 wt% [18] to 25 wt% [3]) for the particle volume fraction. The conditions of the slag production have a significant effect on this value.

2.4. Variable parameters

The effects of the solid-liquid interfacial energies and the perimeter per area of the particle were investigated in the present simulations. The reference system has a system size of [256 256 1], with a slag with initial supersaturation of $x_i = 0.63$ and a particle of 100 by 50 grid points, unless stated otherwise. According to the lever rule, the metal fraction for this x_i is then 0.271 and industrial metal fractions in slags are of the order of 5 % after decantation. But in this model, the minimal value of the metal fraction for a composition within the spinodal region is 0.211. The reference simulation time is 10^6 time steps.

2.4.1. Effect of S-L interfacial energy

Because the solid is assumed not to react and its composition equals the constant x_S , this parameter can be used to adapt the interfacial energy. The composition of the solid particle determines the value of the solid-liquid interfacial energies and thus, for a given $\gamma_{LO,LM}$, the contact angle, as described by Young's equation (7)

$$\gamma_{S,LO} = \gamma_{S,LM} + \gamma_{LO,LM} \cos \theta \quad (7)$$

The effect of the value of x_S on the solid-liquid interfacial energies and the contact angle is demonstrated in Table 2.

Table 2: Variation in x_S , the corresponding variation in the interfacial S-L energies and in the contact angle θ

x_S	$\gamma_{S,LO}$ (N/m)	$\gamma_{S,LM}$ (N/m)	$\gamma_{LO,LM}$ (N/m)	$\theta(^{\circ})$
0.4	1.2641	4.0093	0.903	/
0.5	1.2500	2.8140	0.903	/



0.6	1.2641	2.0260	0.903	147.538
0.7	1.3631	1.5604	0.903	102.621
0.74	1.4455	1.4455	0.903	90.000
0.8	1.6318	1.3325	0.903	70.643
0.9	2.1551	1.2572	0.903	6.092
0.95	2.5387	1.2504	0.903	/

Non-wetting is expected for $x_S \leq 0.57$, a low wettability corresponding to $90^\circ \leq \theta \leq 180^\circ$ for x_S between 0.58 and 0.74, a high wettability corresponding to $0^\circ \leq \theta \leq 90^\circ$ for x_S between 0.74 and 0.90 and full wetting with a non-existing contact angle for x_S -values higher than 0.9.

2.4.2. Effect of perimeter/area

Several length/width ratios are used to investigate the influence of the perimeter per area, while the area of the particle remains constant and has a value of 2400 grid points, corresponding to a particle volume fraction of 0.0366.

Table 3: Variation of the length/width ratio and the corresponding variation in perimeter while maintaining a constant area

Length (grid points)	Width (grid points)	Area (A) (grid points)	Perimeter (P) (grid points)
50	48	2400	192
60	40	2400	196
80	30	2400	216
160	15	2400	346

2.5. Initialisation

At the start of the simulation, the variables have sharp steps at the interfaces. A very small value of L is required because the particle is assumed to not react in these simulations. However, to allow the interface to become diffuse, a larger value of L is used during the first 1000 time steps (Table 1 **Error! Reference source not found.**).

The spinodal decomposition used in this model provides metallic droplets in the initial microstructure, but it should be noted that it is not known whether spinodal decomposition is the real formation mechanism for the metal droplets in slags. Thus, only the growth of the droplets, not their nucleation, can be interpreted physically in the simulations. It was verified that the conclusions on the growth behaviour described in this paper were also found using an alternative nucleation mechanism of the droplets.



2.6. Numerical implementation

A commercial software package Matlab 8.1 (R2013a) [19] was used for all data processing and the semi-implicit Fourier spectral method [20] was employed to solve the kinetic equations numerically.

2.7. Post-processing

Quantitative results were obtained as the area of metallic phase attached to a particle and the fraction of metallic phase attached to the particle. A metal droplet is defined as the connected domain for which $0.71 < x_M - \phi x_S$ holds. To investigate the attachment of the droplets to the solid particle, the droplet (defined as $0.71 < x_M - \phi x_S$) was enlarged with two grid point layers around the droplet and the particle (defined as $0.5 < \phi$) with three grid point layers. When these extended domains overlap, the droplets are considered to be ‘attached’. The total area of the attached droplets is determined as the number of grid points located within attached droplets and multiplied by Δx^2 . The fraction of attached metal is defined as the ratio of the total area of the attached droplets to the total area of metal droplets in the system (equation (16)).

$$f_{\text{attached metal}} = \frac{A_{\text{attached metal}}}{A_{\text{metal total}}} \quad (8)$$

Moreover, contour plots of $x_M - \phi x_S = 0.71$ were obtained at different times during the simulations, to illustrate the evolution of the microstructure.

2.8. Accuracy

Several simulations were performed four times to investigate the spread of the results. The average and standard deviation of the results at the last time step were calculated. Standard deviations for the area and fraction of attached metal are at least one order of magnitude smaller than the average value. The graphs in the results section display error bars corresponding to the abovementioned standard deviations. This value is only significant when wetting occurs. Thus, if wetting occurs, the maximum value of the standard deviation for every wetting regime was plotted.

3. Results and discussion

3.1. General observations

A solid particle changes the behaviour of the spinodal decomposition taking place in the surrounding liquid: three stages can be recognized, which are shown in Figure 2 for a solid particle with $x_S = 0.60$ in a system of size $[512 \ 512 \ 1]$ with an initial supersaturation of $x_i = 0.63$. First, localized spinodal decomposition takes place near the particle, as shown in Figure 2c-d. Secondly, the remaining



supersaturated liquid also decomposes spinodally but in a non-localized way. This is visible in the corners of Figure 2d. Finally, Ostwald ripening (i.e., the growth of larger droplets and dissolution of smaller droplets, as indicated by the black arrows in Figure 2e and g) and coalescence (i.e., the merge of two droplets, as indicated by the black circles in Figure 2f) take place.

Generally, the droplets were attached at various places on the particle with several configurations and varying in time. In this study the main focus was the final values of attached metal fractions in the simulations at a certain simulation time, situated in the coarsening regime.

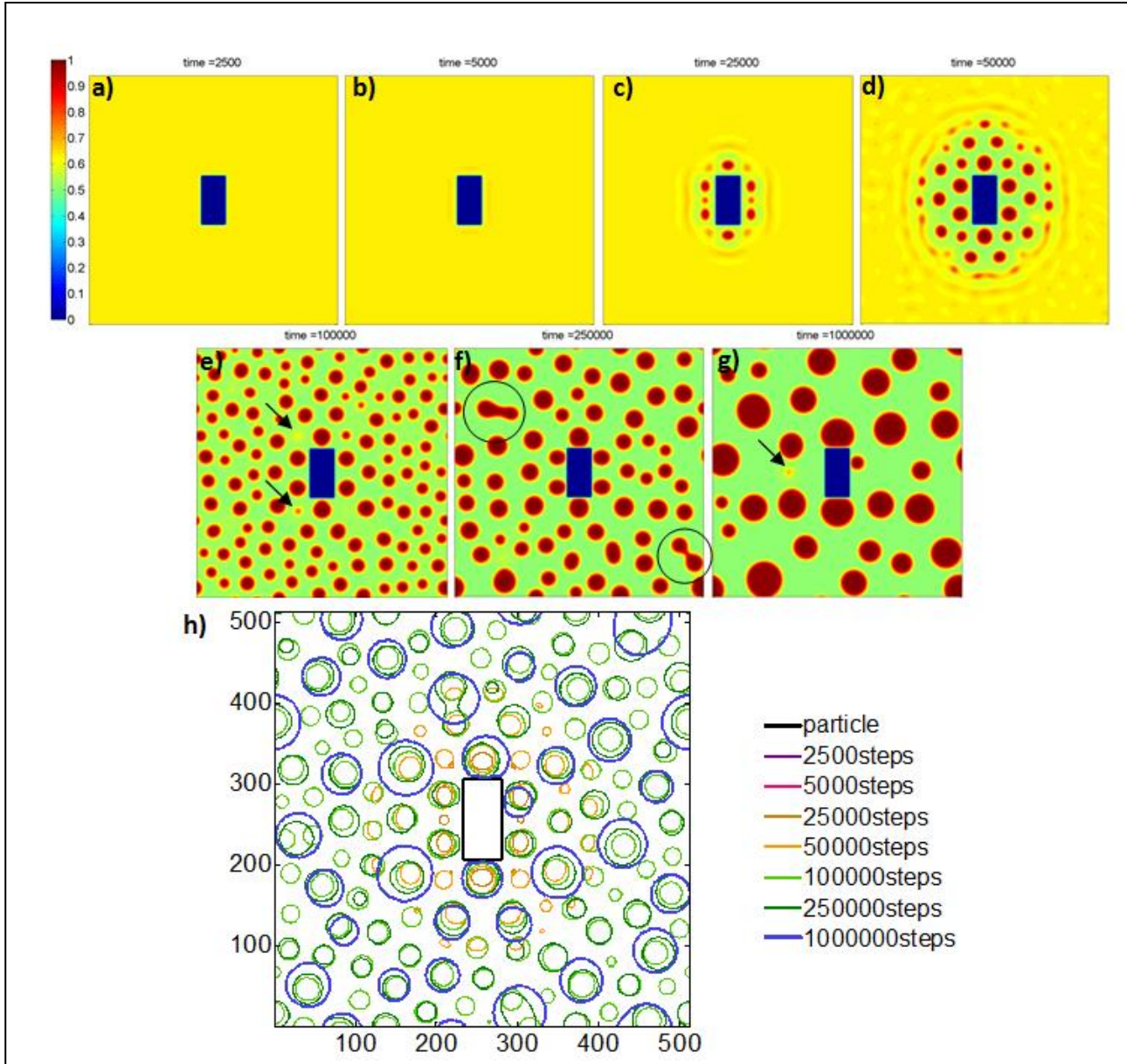


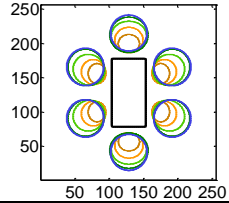
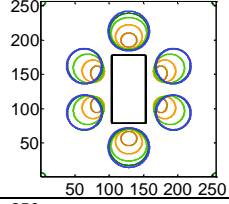
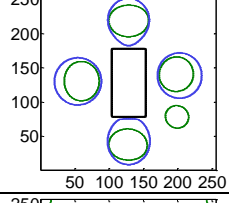
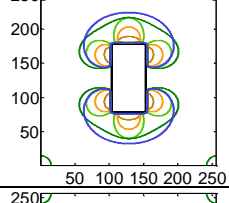
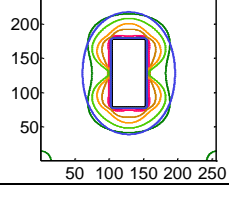
Figure 2: Illustration of the different stages in the spinodal decomposition near a solid particle at different time steps for the simulation with $x_i=0.63$ and $x_s=0.60$ in a system of size $[512 \ 512 \ 1]$ (a-g) with plots of $x_m - \phi \cdot x_s$, scaled to the interval $[0 \ 1]$ such that values lower/higher than the minimum/maximum value are converted to the

minimum/maximum. The particle (defined as $0.5 < \phi$) appears as a blue rectangle. (h) A summary of this in a series of contour plots of $x_M - \phi \cdot x_S = 0.71$ (definition of metal droplets) at different time steps with the corresponding legend on the right (this legend will be the same throughout this paper)

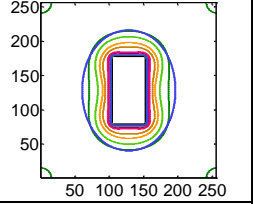
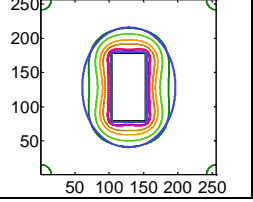
3.2. Effect of S-L interfacial energy

The variation of the parameter x_S was used to study the effect of the solid-liquid interfacial energies on the attachment of the droplets to the particle (see equation 6). The predicted interfacial energies, contact angles and subdivision in wetting regimes, together with the contour plots at time step 10^6 for the systems with x_i -values of 0.61 are shown in Table 4.

Table 4: Influence of the x_S -value on the interfacial energies, predicted contact angle and wetting behaviour, illustrated by contour plots for $x_i=0.61$

x_S	$\gamma_{S,LO}$ (N/m)	$\gamma_{S,LM}$ (N/m)	$\gamma_{LO,LM}$ (N/m)	θ (°)	Wetting behaviour	Contour plots for $x_i=0.61$
0.4	1.2641	4.0093	0.903	/	Non-wetting: only oxide attached	
0.5	1.2500	2.8140	0.903	/	$ \gamma_{S,LO} - \gamma_{S,LM} > \gamma_{LO,LM}$ & $\gamma_{S,LO} < \gamma_{S,LM}$	
0.6	1.2641	2.0260	0.903	147.538	Low wettability: predominantly oxide attached	
0.7	1.3631	1.5604	0.903	102.621	$ \gamma_{S,LO} - \gamma_{S,LM} < \gamma_{LO,LM}$ & $\gamma_{S,LO} < \gamma_{S,LM}$	
0.8	1.6318	1.3325	0.903	70.643	High wettability: predominantly metal attached $ \gamma_{S,LO} - \gamma_{S,LM} < \gamma_{LO,LM}$	



0.9	2.1551	1.2572	0.903	6.092	$\& \gamma_{S,LO} > \gamma_{S,LM}$	
0.95	2.5387	1.2504	0.903	/	Full wetting: only metal attached $ \gamma_{S,LO} - \gamma_{S,LM} > \gamma_{LO,LM}$ $\& \gamma_{S,LO} > \gamma_{S,LM}$	

Generally, a lower contact angle results in an increasing amount of attached metal and two features seem to influence the behaviour of the droplets: Ostwald ripening due to the Gibbs-Thomson effect and an effect due to the interfacial energies between the solid and the different liquids. Four different wetting behaviours are observed.

- Non-wetting: non-existing θ or $\theta = 180^\circ$ ($x_S \leq 0.58$).
The liquid oxide is preferentially attached to the solid instead of the metallic liquid phase, because $\gamma_{S,LO}$ is much smaller than $\gamma_{S,LM}$. Furthermore, the absolute value of the difference between these two S/L interfacial energies is larger than 0.903 (the value of $\gamma_{LO,LM}$), resulting in a non-existing contact angle, i.e. only liquid oxide is attached to the solid particle.
- Low wettability: $90^\circ \leq \theta \leq 180^\circ$ ($x_S = 0.58 - 0.74$)
 $\gamma_{S,LM}$ remains the larger quantity, which still favours the attachment of liquid oxide to the particle, but to a lesser extent because the absolute value of the difference between $\gamma_{S,LO}$ and $\gamma_{S,LM}$ becomes smaller than 0.903. Thus, only a small fraction of the particle's surface is covered by metallic droplets.
- High wettability: $0^\circ \leq \theta \leq 90^\circ$ ($x_S = 0.74 - 0.90$)
The $\gamma_{S,LM}$ value becomes smaller than $\gamma_{S,LO}$ and thus the metallic liquid is preferentially attached to the solid, but the absolute value of the difference between $\gamma_{S,LO}$ and $\gamma_{S,LM}$ remains smaller than 0.903, resulting in the majority of the particle's surface being wetted by metallic droplets.
- Full wetting ($x_S > 0.90$)
The absolute value of the difference between $\gamma_{S,LO}$ and $\gamma_{S,LM}$ is larger than 0.903 and $\gamma_{S,LO}$ is the larger one of the two. Thus, a metal layer forms on the solid.

3.3.Effect of perimeter/area

The aspect ratio of the rectangular particle is changed to investigate the influence of the perimeter per area on the attachment of the metal. Because the area was kept constant during the simulations, the variation of the perimeter will have the same result as a variation of the perimeter/area.



All these simulations were performed for an initial supersaturation of $x_i = 0.63$ and a composition of the solid particle of $x_s = 0.60$ ($\theta = 147.5^\circ$, corresponding to low wettability) and of $x_s = 0.80$ ($\theta = 70.6^\circ$, corresponding to high wettability) in a system of size [256 256 1]. The results are shown in Figure 3.

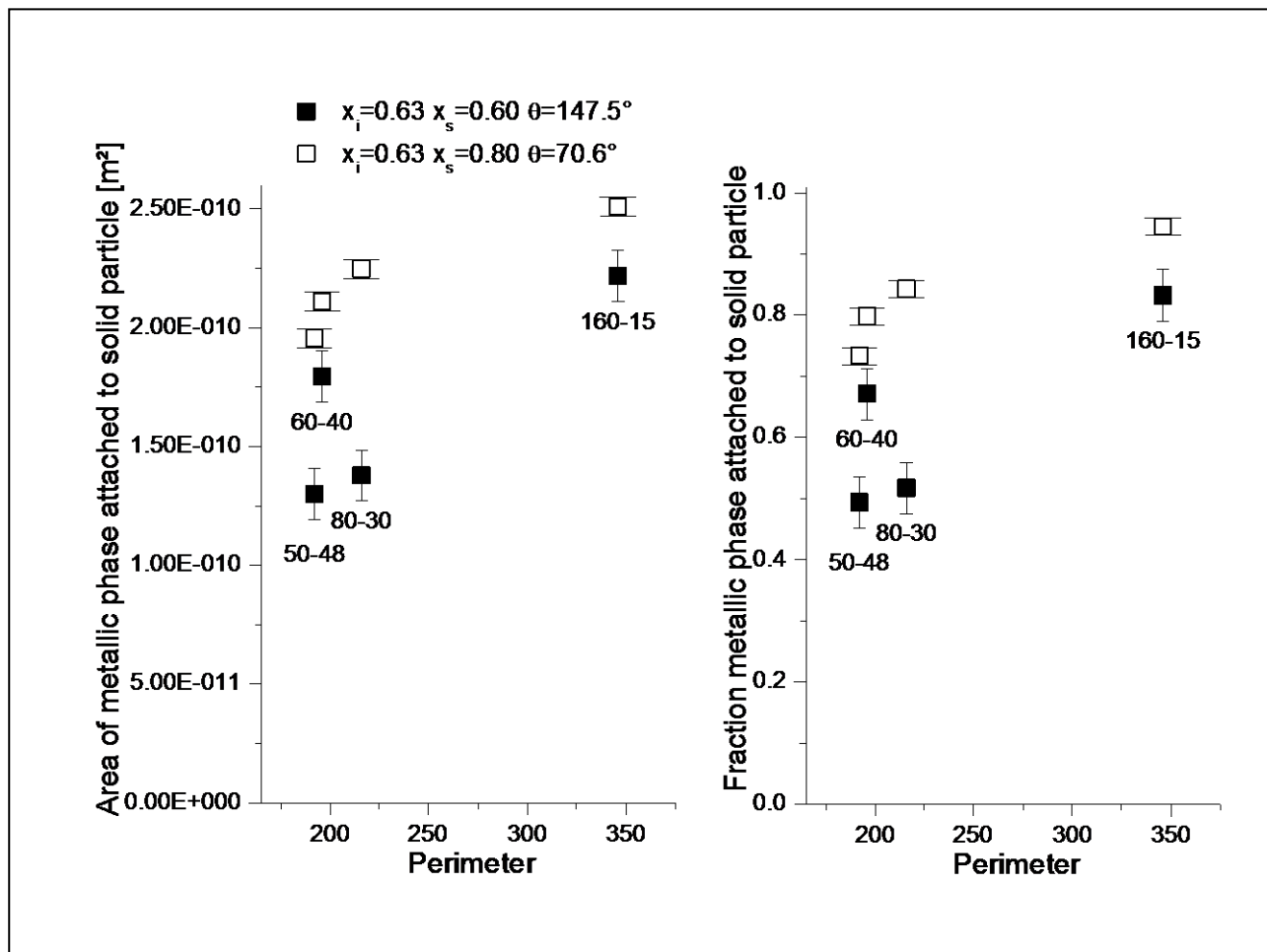


Figure 3: Influence of the perimeter of a rectangular particle on the area and the fraction of the metallic phase attached to the solid for $x_i=0.63$ and $x_s=0.60$ ($\theta=147.5^\circ$) or $x_s=0.80$ ($\theta=70.6^\circ$); the aspect ratios of the rectangles are mentioned as labels to the closed data points; the error bars with the large (small) base correspond to the error made for $x_s=0.80$ (0.60) or the open (closed) symbols.

When the perimeter per area increases, it is expected that a larger amount of metal can be attached to the particle. This is, however, only observed in the case of high wettability ($x_s = 0.80$). As most of the particle's surface is expected to be covered by the metal, the expectations are met. For low wettability, on the contrary, the particle is mostly covered by liquid oxide, resulting in an insignificant influence of the perimeter/area, as indicated by the closed symbols for $x_s = 0.60$.

It should also be mentioned that the shape of the particle has a certain influence: if the shape of the particle is closer to a sphere, e.g. for the rectangular particles investigated in this study this means a



small perimeter, the amount of metal to be attached will be smaller to achieve an energetically preferred spherical shape of the droplet. In contrast, a shape completely different from a sphere, e.g. a stretched rectangular particle, is ‘less spherical’ and thus, more metal is required to achieve the energetically preferred spherical shape of a droplet. This is illustrated in Figure 4.

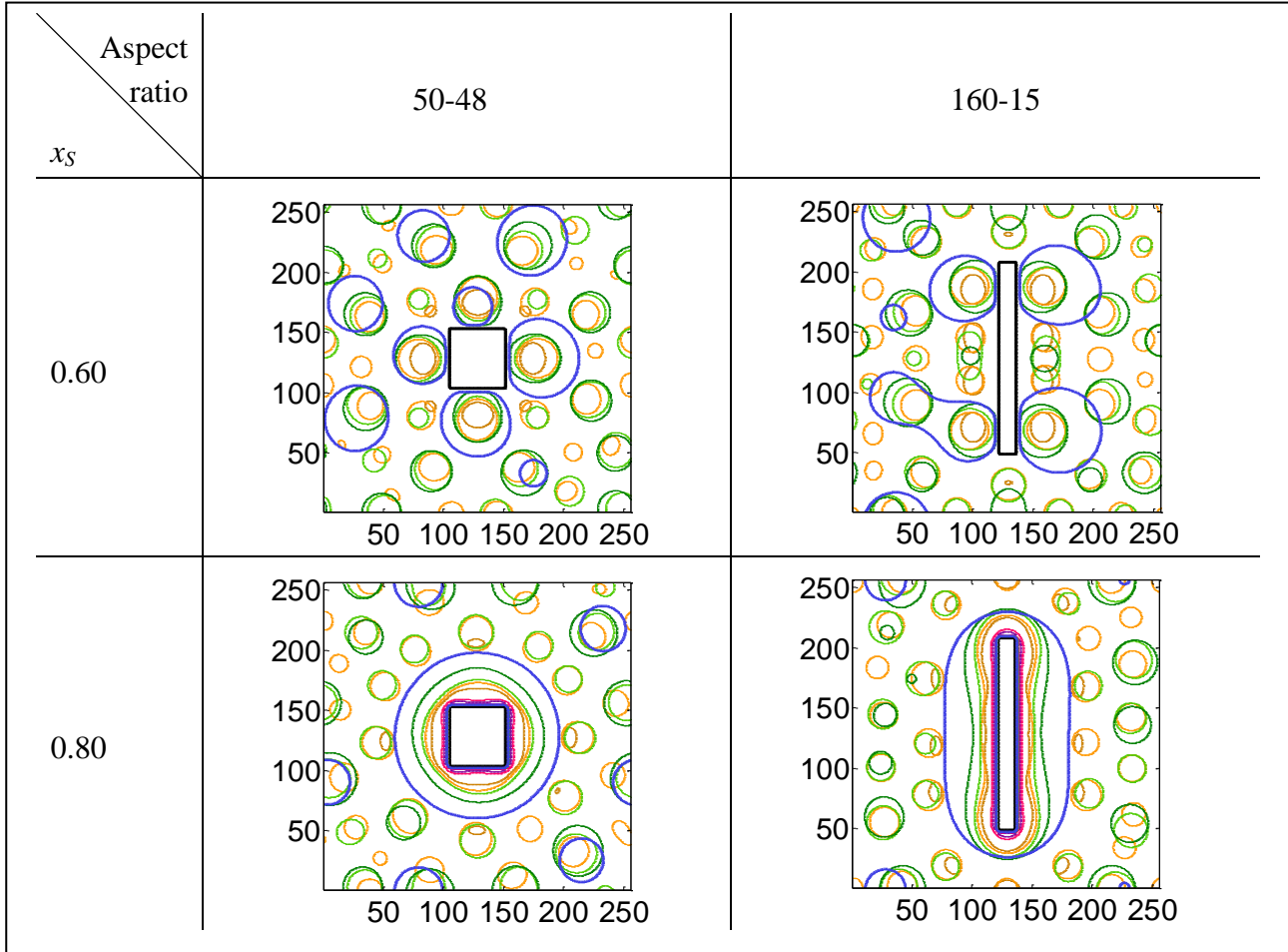


Figure 4: Contour plots of $x_m=0.71$ at different times in the simulations to illustrate the influence of the perimeter per area of the particles on the attachment of the droplets to the particle in low and high wettability regimes

Facetted growth is typical for spinel particles, resulting in particle shapes close to rectangles. Observations of industrial slags and experiments with synthetic slags [21] show that these particles can also possess cavities with a connection to the slag by a channel. Sometimes droplets are found to be present inside these cavities, as shown in Figure 5. This was approximated in simulations, of which the resulting contour plots for both low and high wettability are shown in Figure 6.



Figure 5: Experimentally obtained micrographs of Cu droplets within a cavity inside a solid particle indicated by white circles [21]

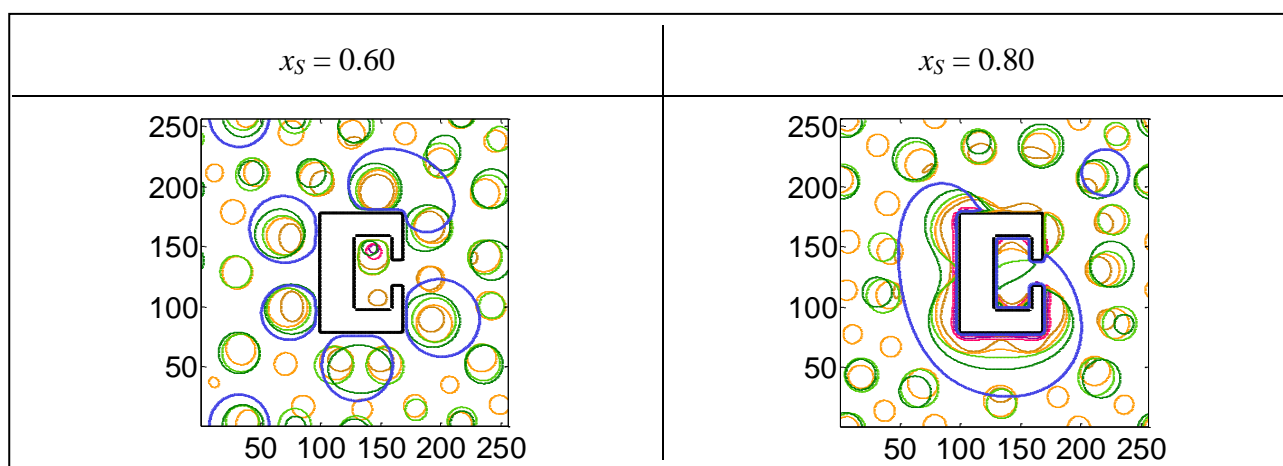


Figure 6: Contour plots of $x_m=0.71$ at different times in the simulations to investigate a cavity and a channel in a particle as an approximation of the experimentally observed particle in Figure 5 in low ($x_S = 0.60$) and high ($x_S = 0.80$) wettability regimes

The cavity has the most influence in the case of high wettability: the droplet first grows inside the cavity, which then restricts further growth of the droplet. Thus the cavity provides the particle with a large perimeter per area but in the meantime it also limits the amount of attached metal. Thus, the amount of attached metal is relatively low for such a large perimeter/area ratio in the case of high wettability. In contrast, for low wettability: if a droplet is formed inside the cavity, it is either trapped there or it dissolves again and the amount of attached metal is only slightly lower for such a large perimeter/area. Therefore, an important conclusion is that not only the perimeter, but also the space available for the droplet to grow is important.



4. Conclusions

In industry, when a fraction of the metallic phase is attached to the solid particles in the slag, this fraction cannot settle and the yield of the phase separation will decrease, which in turn means an important loss of valuable metals.

This study investigates the influences of the interfacial energies and the particle perimeter per area on the attachment of liquid metal droplets to solid particles in liquid slags with a phase field model. This model describes a two-phase solid-liquid system with spinodal decomposition in the liquid. The solid particles do not react with the liquid.

Spinodal decomposition near a solid particle takes place in three stages: first, ‘localized’ spinodal decomposition in the proximity of the particle, then, non-localized decomposition in the remaining supersaturated liquid and finally, Ostwald ripening and coalescence.

Four wetting regimes were obtained with the variation of the interfacial energies: no wettability of the metal on the particle, low wettability, high wettability and full wetting.

The perimeter influences the amount of attached metal in the case of high wettability, but not for low wettability. Moreover, the available space for the droplet growth is an important factor. This study indicates that better phase separations in a high wettability regime would result from fewer, but larger solid particles close together.

The solid particles and metallic droplet interacted by differences in interfacial energies, in this study, but actually chemical reactions between the solid and the two liquid phases are possible. This could be incorporated in the model in future investigations.

Acknowledgments

I. Bellemans holds a Ph. D. fellowship of the Research Foundation - Flanders (FWO). Part of this work has been done in the framework of the bachelor thesis of E. Vranken.

References

- [1] R. Sridhar, J. M. Toguri, and S. Simeonov, “Copper losses and thermodynamic considerations in copper smelting,” *Metall. Mater. Trans. B*, vol. 28, no. 2, pp. 191–200, Apr. 1997.
- [2] F. A. Calvo and A. Ballester, “The settling of metallic lead from lead blast furnace slag,” *Metall. Trans. B*, vol. 17, no. 2, pp. 267–270, Jun. 1986.
- [3] E. De Wilde, I. Bellemans, S. Vervynckt, M. Campforts, K. Vanmeensel, N. Moelans, and K. Verbeken, “Towards a methodology to study the interaction between Cu droplets and spinel particles in slags,” in *Proceedings of EMC 2013*, Weimar, Germany, 2013, vol. 1.
- [4] A. Karma and W.-J. Rappel, “Quantitative phase-field modeling of dendritic growth in two and three dimensions,” *Phys. Rev. E*, vol. 57, no. 4, pp. 4323–4349, Apr. 1998.



- [5] J. Heulens, B. Blanpain, and N. Moelans, "A phase field model for isothermal crystallization of oxide melts," *Acta Mater.*, vol. 59, no. 5, pp. 2156–2165, Mar. 2011.
- [6] L.-Q. Chen, "Phase-Field Models for Microstructure Evolution," *Annu. Rev. Mater. Res.*, vol. 32, no. 1, pp. 113–140, 2002.
- [7] Y. U. Wang, "Computer modeling and simulation of solid-state sintering: A phase field approach," *Acta Mater.*, vol. 54, no. 4, pp. 953–961, Feb. 2006.
- [8] N. Moelans, B. Blanpain, and P. Wollants, "An introduction to phase-field modeling of microstructure evolution," *Calphad*, vol. 32, no. 2, pp. 268–294, Jun. 2008.
- [9] I. Bellemans, N. Moelans, and K. Verbeken, "Phase field modelling of the attachment of metallic droplets to solid particles in liquid slags: influence of interfacial energies and slag supersaturation," *Comput. Mater. Sci.*, accepted.
- [10] I. Bellemans, N. Moelans, and K. Verbeken, "Phase field modelling of the attachment of metallic droplets to solid particles in liquid slags: the influence of particle characteristics," to be submitted.
- [11] M. Hillert, "A Theory of Nucleation of Solid Metallic Solutions," Mass. Inst. Tech, 1956.
- [12] J. W. Cahn and J. E. Hilliard, "Free Energy of a Nonuniform System. I. Interfacial Free Energy," *J. Chem. Phys.*, vol. 28, no. 2, p. 258, Feb. 1958.
- [13] J. W. Cahn and J. E. Hilliard, "Free Energy of a Nonuniform System. III. Nucleation in a Two-Component Incompressible Fluid," *J. Chem. Phys.*, vol. 31, no. 3, pp. 688–699, 1959.
- [14] S. M. Allen and J. W. Cahn, "A microscopic theory for antiphase boundary motion and its application to antiphase domain coarsening," *Acta Metall.*, vol. 27, no. 6, pp. 1085–1095, Jun. 1979.
- [15] T. Sakai, S. W. Ip, and J. M. Toguri, "Interfacial phenomena in the liquid copper-calcium ferrite slag system," *Metall. Mater. Trans. B*, vol. 28, no. 3, pp. 401–407, Jun. 1997.
- [16] H. Sun, K. Nakashima, and K. Mori, "Influence of Slag Composition on Slag-Iron Interfacial Tension," *ISIJ Int.*, vol. 46, no. 3, pp. 407–412, 2006.
- [17] N. Moelans, "A quantitative and thermodynamically consistent phase-field interpolation function for multi-phase systems," *Acta Mater.*, vol. 59, no. 3, pp. 1077–1086, Feb. 2011.
- [18] S. Mostafaei, M. Andersson, and P. Jönsson, "Petrographic and thermodynamic study of slags in EAF stainless steelmaking," 18-Jul-2013. .
- [19] *Matlab 7.12.0 (R2011a)*. Natick, MA: The MathWorks Inc., 2011.
- [20] L.-Q. Chen and J. Shen, "Applications of semi-implicit Fourier-spectral method to phase field equations," *Comput. Phys. Commun.*, pp. 147–158, 1998.
- [21] E. De Wilde, I. Bellemans, M. Campforts, K. Vanmeensel, M. Guo, A. Rhamdhani, G. Brooks, A. Khaliq, B. Blanpain, N. Moelans, and K. Verbeken, "The wetting behaviour of Cu-based alloys on spinel substrates in a pyrometallurgical context," *Mater. Sci. Technol.*, submitted.